ENCIT 2018

ABCM Associação Brasileira de Engenharia e Ciências Mecânicas

17th Brazilian Congress of Thermal Sciences and Engineering
November 25th-28th, 2018, Águas de Lindóia, SP, Brazil

ENCIT-2018-0305
Computational Study of Heat Transfer in an Asymmetrical Natural Circulation Circuit with Heat Generation

Ian Boshoff
Jian Su
PEN-COPPE/UFRJ
ianboshoff@gmail.com

Abstract. *This paper aims to study and model the natural circulation on an asymmetrical circuit with heat generation in only one side. The effects of different turbulence models and mesh refinements were analyzed in order to determine the optimal RANS simulation parameters. Since the circuits had important regions of free flow and near the walls, the SST turbulence model showed better performance. Several conditions of heat generation were studied to determinate an equation relating the Nusselt number and the Rayleigh number. The results obtained proved to be very close to natural circulation circuits with more rectangular geometries and different heat sources.*

Keywords: *Turbulence Models, Natural Circulation, RANS, Heat Generation, CFD*

1. INTRODUCTION

Molten Salt Reactors(MSR) were first introduced in the late 1940, with the concept of using a mixture of molten salts containing fissile and fertile isotopes dissolved as fuel, and also serving as a heat transfer medium. The fluidity of the fuel offers great advantages both to security and to its heat transference. Because of the uneven heat generation inside the fluid core of a MSR, natural circulation is an interesting phenomenon to study in this kind of reactor.

The use of passive operational methods such as natural circulation increases the reliability and is a highly desirable practice and thus should be used when appropriate IAEA (1991). The reactor in this study aims to be as reliable as possible, using both the natural circulation and a fluid under nuclear fission, based on the EVOL project design.

Since there are no experimental studies combining natural circulation and the desired characteristics of a MSR, we used experimental data extrapolated from circuits as close to ours as possible. For instance, Barozzi (2000) studied the natural circulation in a square cavity with an obstacle in the center, in a fluid with heat generation and fixed temperatures on the sides. Nishikawa (2015) studied experimentally with natural circulation in a rectangular loop, keeping the cold walls at a fixed temperature and changing the heat rate received in the hot side. The study modeled Nusselt number as a function of the Rayleigh Number.

We compared our simplification of a Molten Salt Fast Reactor(MSFR) results with the experimental results from those studies in order to have better estimative of the natural circulation under those circumstances.

2. METHODOLOGY

We based our studies in a reactor proposed by the Evaluation and Viability of Liquid Fuel Fast Reactor System (EVOL) project as described by Brovchenko (2012), a fast reactor that uses molten thorium salt as its fuel. In order to broaden the scope of our study and make it closer to the experimental conditions, we used a 2D projection of the reactor proposed by the EVOL project with constant heat generation only on its core.

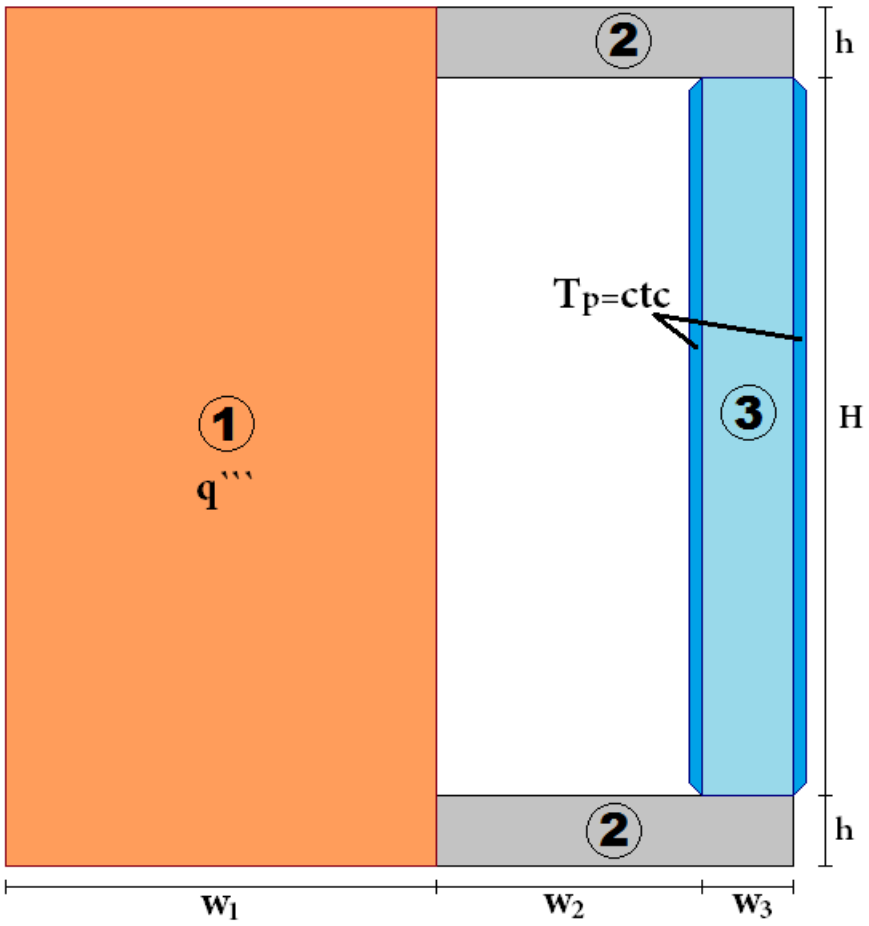

Figure 1: Diagram of the Natural Circulation Circuit simulated.

Figure 1 shows the simplifications and the dimensions used in this study. Region 1 represents the reactor core, and thus is simulated as a uniform heat generation (q'''), Region 2 is a transitional area between the hot and the cold areas and Region 3 represents the heat removal system, having its walls cooled to a constant temperature (T_p).

2.1 Balance Equations

In order to represent our system, we used the following equations:

$$\frac{\partial \rho}{\partial t} + \nabla \cdot (\rho \mathbf{U}) = 0 \tag{1}$$

Equation (1) represents the mass balance for an incompressible fluid in a transient regime, which is only used to get a easier to converge step for the steady state. In the Steady State, all of the transient terms, such as $\frac{\partial \rho}{\partial t}$ are removed from the equations.

$$\frac{\partial \mathbf{U}}{\partial t} + \nabla \cdot (\mathbf{U}\mathbf{U}) + divDevReff(\mathbf{U}) = -(\mathbf{g} \cdot \mathbf{r}) \nabla \rho_k - \nabla \tilde{P}_{rgh} \tag{2}$$

The momentum balance is written in Eq. (2), while the term $divDevReff(\mathbf{U})$ is given by equation Eq. (3) and ρ_k by equation Eq. (4).

$$divDevReff(\mathbf{U}) = -\nabla \cdot (\nu_{Eff} \nabla \mathbf{U}) - \nabla \cdot \left\{ \nu_{Eff} \left[(\nabla \mathbf{U})^T - \frac{1}{3} trace \left[(\nabla \mathbf{U})^T \right] I \right] \right\} \tag{3}$$

The term ν_{Eff} is defined by the turbulence model, which will be detailed in the next subchapter.

$$\rho_k = \frac{\rho}{\rho_0} = 1 - \beta\left(T - T_{ref}\right) \tag{4}$$

T_{ref} is used as the same value as T_p since the heat generation is not significant and the temperature distribution in the fluid is not too far from the wall temperature. The temperatures are given by the energy balance:

$$\frac{\partial T}{\partial t} + \nabla \cdot (T\mathbf{U}) - \nabla \cdot \alpha_{Eff} \nabla T = \frac{q'''}{\rho_0 c_P} \tag{5}$$

α_{Eff} is calculated using ν_{Eff}, which is given by the turbulence model:

$$\alpha_{Eff} = \alpha + \alpha_T = \frac{\nu}{Pr} + \frac{\nu_T}{Pr_T} \tag{6}$$

2.2 Turbulence Models

The RANS equations introduces the average of the products of the fluctuating velocity, a symmetrical tensor which is not determined by the usual balances, and thus has to be modelled using a turbulence model. Kolmogorov (1942) proposed the modelling of this tensor as:

$$-\overline{u_i' u_j'} = \nu_t \left(\frac{\partial \overline{u_i}}{\partial x_j} + \frac{\partial \overline{u_i}}{\partial x_j} \right) + \frac{2}{3}\kappa \delta_{ij} \tag{7}$$

with κ being the Kinetic turbulence energy:

$$\kappa = \frac{1}{2}\overline{u_i' u_i'} \tag{8}$$

This kind of modelling reduces the problem from the 6 variables in the Reynolds stress tensor to only 2 variables, ν_t and κ, and thus are often referred as turbulent viscosity models Launder and Spalding (1974).

2.2.1 Kappa-Epsilon

Kappa-Epsilon describes ν_t as a function of κ and a parameter ϵ. For high Reynolds Numbers, these parameters are given by A. P. S. Freire and Colaço (2006):

$$\frac{\partial \kappa}{\partial t} + \overline{u_j}\frac{\partial \kappa}{\partial x_j} = \frac{\partial}{\partial x_j}\left[\left(\nu + \frac{\nu_t}{\sigma_\kappa} \right) \frac{\partial \kappa}{\partial x_i} \right] + \left[\nu_t \left(\frac{\partial \overline{u_i}}{\partial x_j} + \frac{\partial \overline{u_j}}{\partial x_i} \right) - \frac{2}{3}\kappa \delta_{ij} \right] - \varepsilon \tag{9}$$

$$\frac{\partial \varepsilon}{\partial t} + \overline{u_j}\frac{\partial \varepsilon}{\partial x_j} = \frac{\partial}{\partial x_j}\left[\left(\nu + \frac{\nu_t}{\sigma_\varepsilon} \right) \frac{\partial \kappa\varepsilon}{\partial x_i} \right] + C_{\varepsilon 1}\frac{\varepsilon}{\kappa}\left[\nu_t \left(\frac{\partial \overline{u_i}}{\partial x_j} + \frac{\partial \overline{u_j}}{\partial x_i} \right) - \frac{2}{3}\kappa \delta_{ij} \right] \frac{\partial \overline{u_i}}{\partial x_j} - C_{\varepsilon 2}\frac{\varepsilon^2}{\kappa} \tag{10}$$

$$\nu_t = C_\mu \frac{\kappa^2}{\epsilon} \tag{11}$$

2.2.2 Kappa-Omega

Although similar to the $\kappa - \epsilon$, this model introduces the parameter ω, which means a rate of turbulent kinetic energy dissipation divided by the turbulent kinetic energy.

$$\frac{\partial \kappa}{\partial t} + \overline{u_j}\frac{\partial \kappa}{\partial x_j} = \frac{\partial}{\partial x_j}\left[\left(\nu + \frac{\nu_t}{\sigma_{\kappa 1}} \right) \frac{\partial \kappa}{\partial x_j} \right] + \left[\nu_t \left(\frac{\partial \overline{u_i}}{\partial x_j} + \frac{\partial \overline{u_j}}{\partial x_i} \right) - \frac{2}{3}\kappa \delta_{ij} \right] \frac{\partial \overline{u_i}}{\partial x_j} - \beta_\kappa \kappa \omega \tag{12}$$

$$\frac{\partial \omega}{\partial t} + \overline{u_j}\frac{\partial \omega}{\partial x_j} = \frac{\partial}{\partial x_j}\left[\left(\nu + \frac{\nu_t}{\sigma_{\omega 1}}\right)\frac{\partial \varepsilon}{\partial x_j}\right] + \alpha_1 \frac{\omega}{\kappa}\left[\nu_t\left(\frac{\partial \overline{u_i}}{\partial x_j} + \frac{\partial \overline{u_j}}{\partial x_i}\right) - \frac{2}{3}\kappa\delta_{ij}\right]\frac{\partial \overline{u_i}}{\partial x_j} - \beta_{\omega 1}\omega^2 \tag{13}$$

Table 1: Constants used in Kappa-Epsilon and Kappa-Omega models

Kappa-Epsilon	
Constant	Value
C_μ	0.09
σ_κ	1.00
σ_ε	1.30
$C_{\varepsilon 1}$	1.44
$C_{\varepsilon 2}$	1.92

Kappa-Omega	
Constant	Value
α_1	5/9
β_κ	9/100
$\beta_{\omega 1}$	3/40
$\alpha_{\kappa 1}$	2
$\alpha_{\omega 1}$	2

2.2.3 SST

This model tries to solve the kappa-omega sensitivity for free-streams and the kappa-epsilon problems near the walls by combining both to use each on the region where it works best.

$$\Phi_{SST} = F \cdot \Phi_{\kappa-\omega} + (1 - F)\,\Phi_{\kappa-\varepsilon} \tag{14}$$

$$F = tanh\left(min^4\left[max\left(\frac{\sqrt{\kappa}}{\beta_\kappa \omega y}\right), \frac{4\rho\kappa}{max\left(2\rho\frac{1}{\sigma_{\omega 2}\omega}\frac{\partial \kappa}{\partial x_j}\frac{\partial \omega}{\partial x_j}, 10^{-10}\right)\sigma_{\omega 2} y^2}\right]\right) \tag{15}$$

2.3 Computational Method

We used the software OpenFOAM™ to simulate a natural circulation circuit with our desired conditions. The fluid was treated as incompressible, and its density was assumed to be constant except for the buoyancy effect (Bousinessq approximation).

Due to the simplicity of the geometry of our simulation, we opted to use an uniform structured grid mesh for our simulations, and analyze the number of cells we would need in order to accurately describe the physical phenomenon.

2.4 Dimensionless Numbers

In order to make this study comparable with others, we decided to use our calculations using dimensionless numbers as follows:

$$Ra_i = \frac{Pr^2 g \beta H^5 {q_{rhoCp}}'''}{\nu^3} \tag{16}$$

$$Pr = \frac{\nu}{\alpha} \tag{17}$$

$$\frac{q''}{\rho Cp} = \alpha_{Eff}\nabla T \tag{18}$$

$$h = \frac{q''}{(T - T_\infty)} \tag{19}$$

$$Nu = \frac{hL}{k} = \frac{q''L}{\alpha\,(T_m - T_p)} = \frac{L\left(\frac{\partial T}{\partial x}\,|_{w_l} - \frac{\partial T}{\partial x}\,|_{w_r}\right)}{T_m - T_p} \tag{20}$$

3. RESULTS AND DISCUTIONS

The geometrical parameters used to simulate the circuit were:

Table 2: Dimensions of the Natural Circulation Circuit as shown in Fig. 1 Aufiero (2014)

Parameter	**Value(m)**
w_1	1.1275
w_2	0.7000
w_3	0.2370
h	0.1878
H	1.8800

In order to make it easier to compare the results, we will analyze the heat transfer represented by region 3 of Fig. 1, showing its flow lines and velocity, average dimensionless temperature in its cross section and the Nusselt number associated with it.

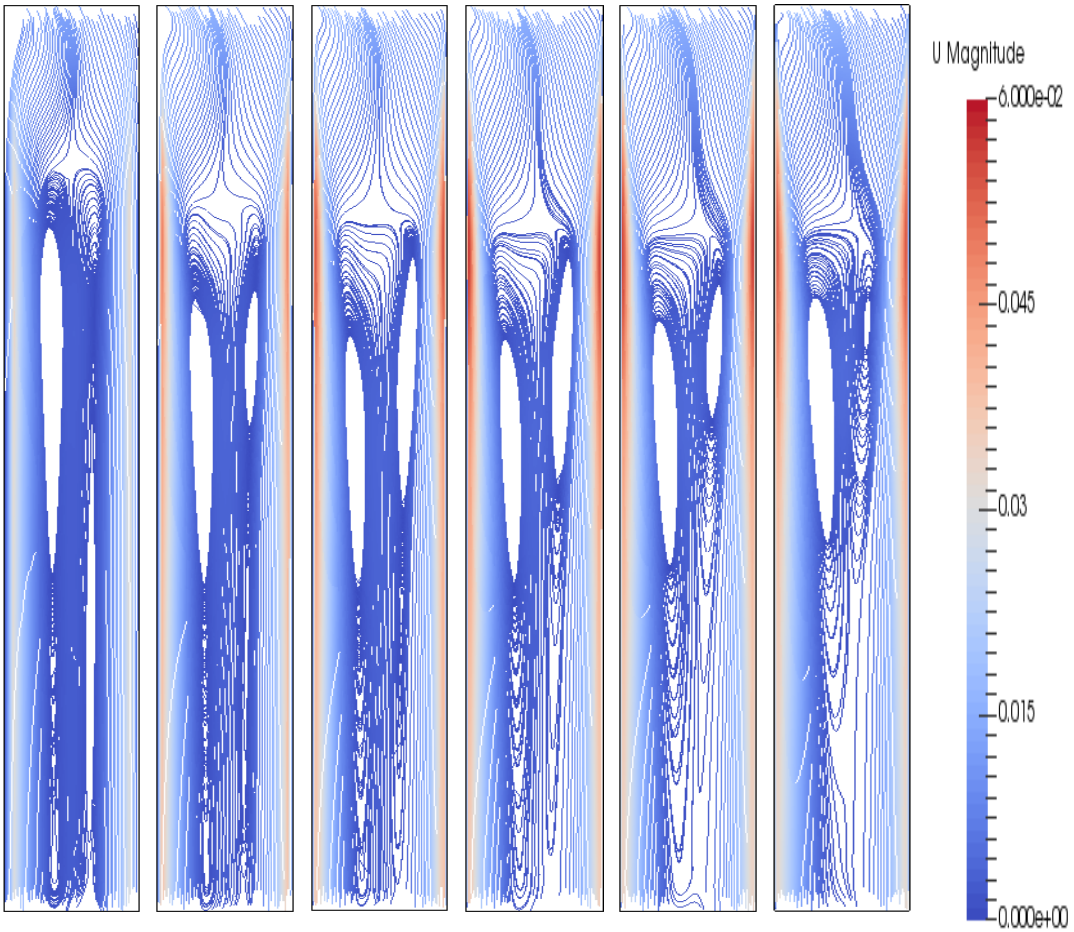

(a) 5068 (b) 20272 (c) 45612 (d) 81088 (e) 182448 (f) 410508

Figure 2: Effect of the mesh refinement on the flow lines, using Kappa-Episilon turbulence model.

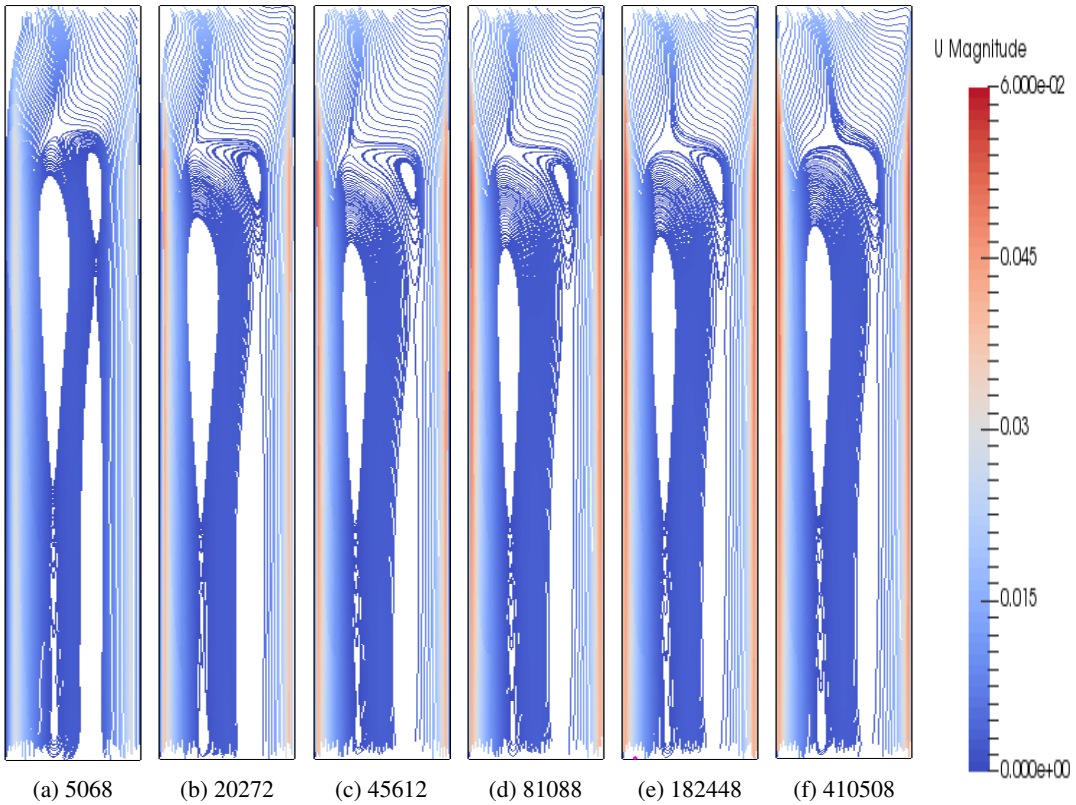

(a) 5068 (b) 20272 (c) 45612 (d) 81088 (e) 182448 (f) 410508

Figure 3: Effect of the mesh refinement on the flow lines, using Kappa-Omega turbulence model.

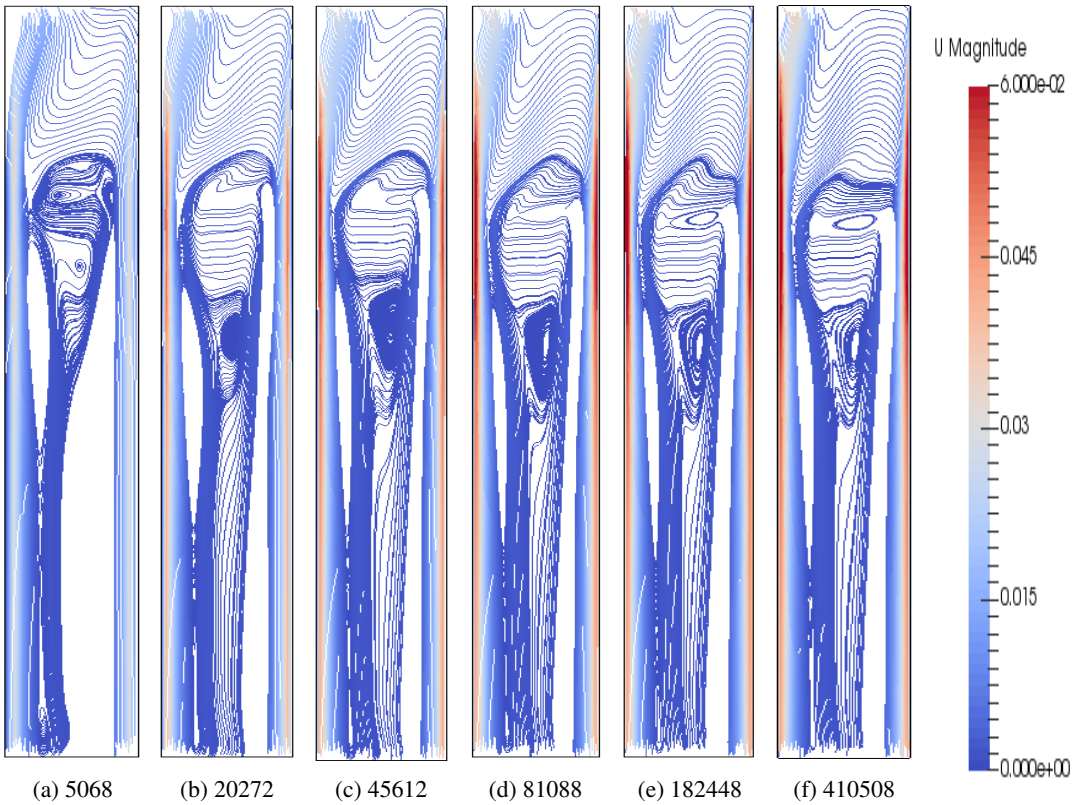

(a) 5068 (b) 20272 (c) 45612 (d) 81088 (e) 182448 (f) 410508

Figure 4: Effect of the mesh refinement on the flow lines, using SST turbulence model.

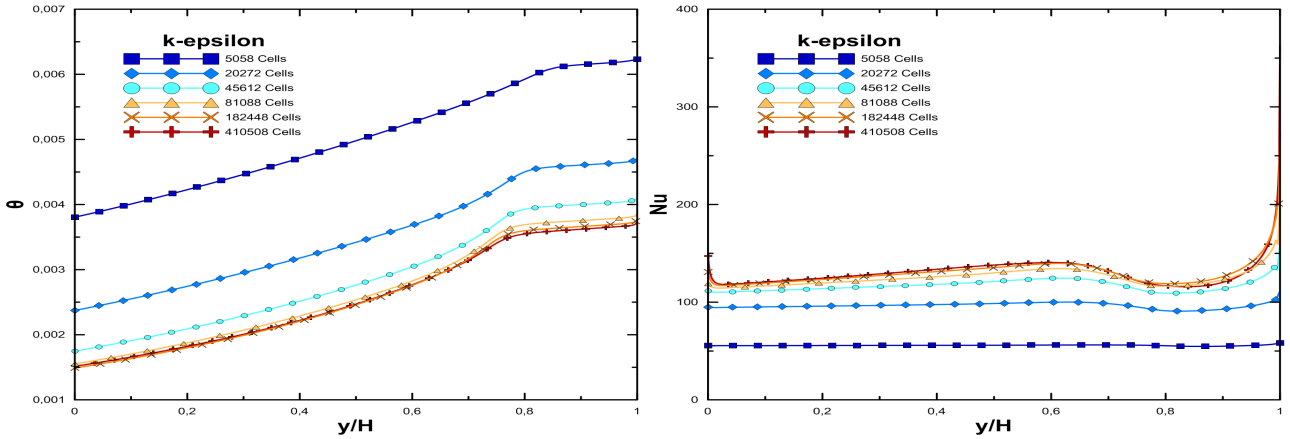

(a) Mean dimensionless temperature on the cooling channel for each mesh refinement.

(b) Nusselt Number on the cooling channel for each mesh refinement.

Figure 5: Effect of the mesh refinement on the mean dimensionless temperature and Nusselt number distribution using the Kappa-Episilon turbulence model.

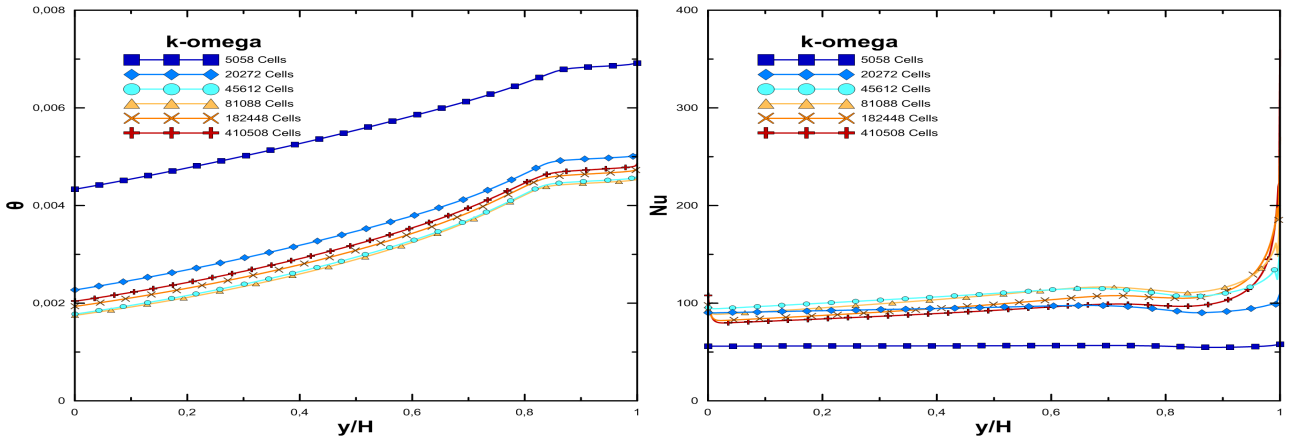

(a) Mean dimensionless temperature on the cooling channel for each mesh refinement.

(b) Nusselt Number on the cooling channel for each mesh refinement.

Figure 6: Effect of the mesh refinement on the mean dimensionless temperature and Nusselt number distribution using the Kappa-Omega turbulence model.

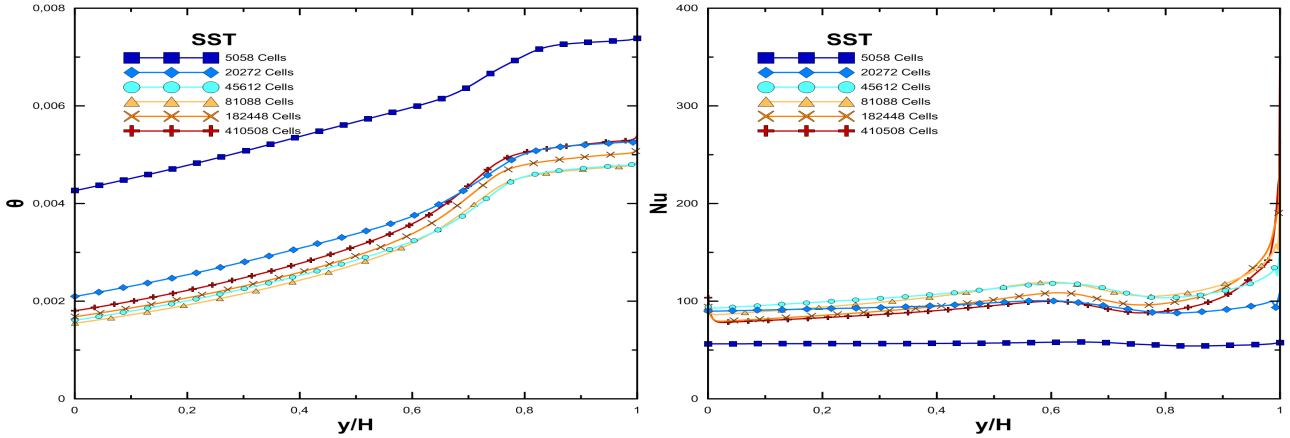

(a) Mean dimensionless temperature on the cooling channel for each mesh refinement.

(b) Nusselt Number on the cooling channel for each mesh refinement.

Figure 7: Effect of the mesh refinement on the mean dimensionless temperature and Nusselt number distribution using the SST turbulence model.

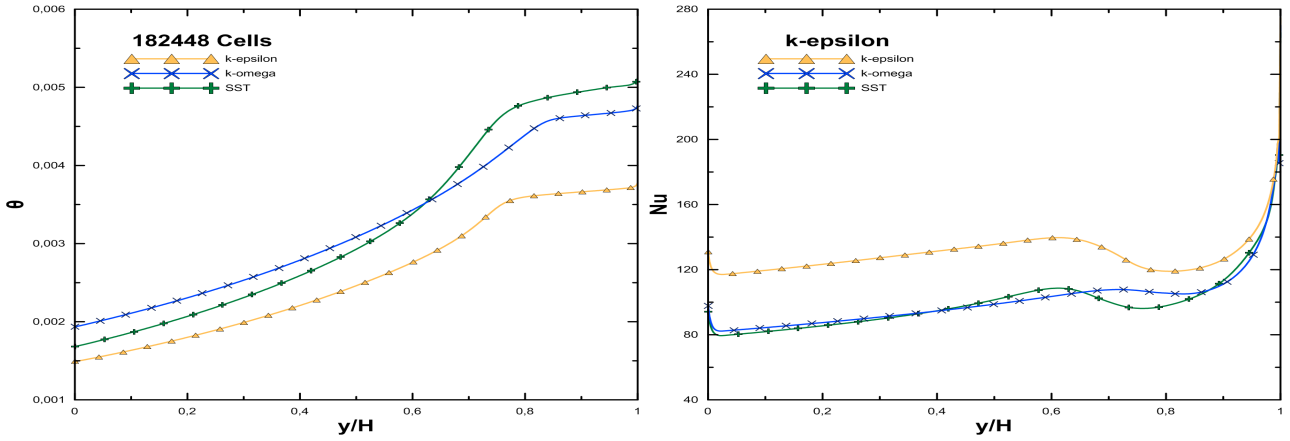

(a) Mean dimensionless temperature on the cooling channel for each turbulence model.

(b) Nusselt Number on the cooling channel for each turbulence model.

Figure 8: Effect of the turbulence model on the mean dimensionless temperature and Nusselt number distribution using the 182448 cells mesh.

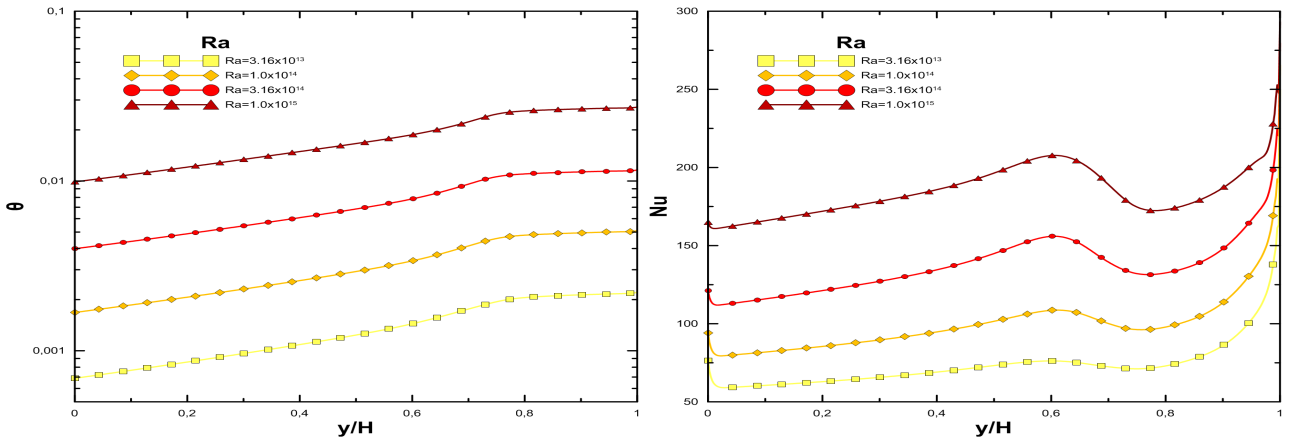

(a) Mean dimensionless temperature on the cooling channel for each Rayleigh number.

(b) Nusselt Number on the cooling channel for each Rayleigh number.

Figure 9: Effect of the Rayleigh number on the mean dimensionless temperature and Nusselt distribution using the 182448 cells mesh and SST turbulence model.

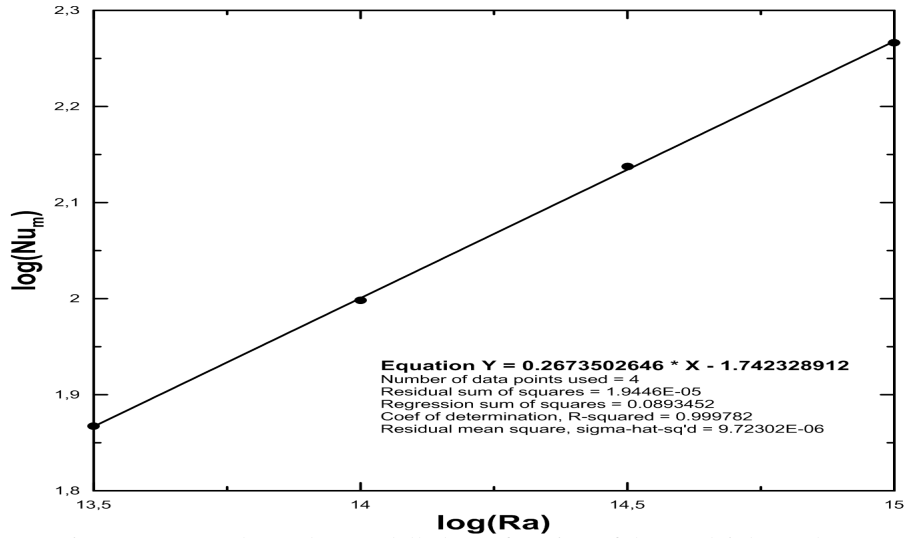

Figure 10: Nusselt number modelled as a function of the Rayleigh number.

$$Nu = 0.0181 \times Ra^{0.2674} \tag{21}$$

By plotting the $log(Nu_m)$ against the $log(Ra)$ and finding the linear curve that best fits the data, we were able to rearrange the formula to get the following relation between the average Nusselt and the Rayleigh number.

3.1 Turbulence models and Mesh Analysis

We can see in Fig. 5, Fig. 6 and Fig. 7 that the mesh with 5028 cells displays dimensionless temperatures very far from the more accurate meshes. Its temperature curve is also way more linear then the other curves, which results in an almost constant Nusselt curve with any of the turbulence models.

As the mesh refinement increases to 20272, 45612 and 81088 cells, the temperature curves get lowered as the simulated problem gets closer to the convergence, and the curvatures get stepper, especially near y/H=0.68. The 45612 and 81088 temperature curves get so close that the bigger curvature on the ladder makes them cross each other both on the kappa-omega and on the SST graphs.

This occurs due to the formation of a vortex around that height, as shown on Fig. 2. Since vorticity can only be generated in the contour, the models that represent the flow around the display this phenomenon more accurately. We can see this as both the kappa-omega and the SST temperature curves cross on the 45612 and 81088 meshes, while the kappa-episilon only crosses between the 182448 and 410508 meshes, struggling to represent the vortex without a lot of refinement.

In these same figures, if we look at Nusselt number curves, we can see that most of the curves show a sharp drop near the top of the channel. This happens due to the angle of the velocity not being close to orthogonal with the cells faces Fig. 2. This results in interpolation errors to the methods, but can be mitigated by using smaller mesh elements and applying corrections. We chose to keep our studies using 182448 mesh, due to its reasonable accuracy compared to the more refined mesh with all of the turbulence models, but requiring way less computational effort than the 410508 mesh.

With our mesh refinement defined, we proceeded to study the turbulence models as show on Fig. 8. Both the curves with kappa-omega and SST turbulence models had close values for temperatures and Nusselt number, while the kappa-omega had lower temperatures and higher Nusselt, but had curves very similar to the SST ones, although shifted.

This seems to indicate that the shape of these curves is related to the free flow accuracy of the turbulence model, after it has passed the vortex. Because it is able to represent well both the vortex region and also the free flow region, we decided to use the SST model to model the Nusselt number as a function of the heat generation.

3.2 Heat transfer modeling

As shown on Fig. 8, we simulated the circuit again for different heat rates, ranging from Rayleigh 3.162×10^{13} to 10^{15}. As expected, both the average temperature and the Nusselt number increased as we increased the Rayleigh number, but so did the sharp drop near the top of the channel. Also, as we got closer 10^{15}, the temperatures started get farther from the limits to use of the boussinesq approximation accurately.

Since the curves showed almost the same characteristics except for the amplitude, the vortex that appeared are probably not very influenced by the heat generation, and are mostly generated due the geometry of the problem. This implies that maybe if we round the corners of the geometry, it would be possible to reduce the vortex or at least make it only appear further down the cooling channel, improving the overall heat transfer.

In Fig. 9, we made a linear regression between $log(Nu_m)$ and $log(Ra)$. Due the R^2 of this approximation being very close to 1, we can propose a model to estimate the heat transfer in this kind of circuit with great accuracy as shown in Eq. (21).

Although we only tested for Pr=1, the exponential of the Rayleigh number is a great indicator of the circulation modeling, being widely studied experimentally for natural circulation circuits similar to ours. For instance, Barozzi (2000) studied a symmetrical cavity with a heat generating obstacle in the center and fixed temperatures on the sides and concluded that the Rayleigh exponent should be $0.25 \leq \alpha \leq 0.33$ for turbulent flows.

Nishikawa (2015) studied natural circulation on a rectangular circuit with fixed cooling temperatures and constant heat flux on the hot walls. The conclusion was that for that geometry, the Rayleigh exponent on the turbulent region was $\alpha = 0.3$.

The value obtained in this study (Eq. 21, $\alpha = 0.2674$) is reasonably close to the experimental data found in the literature, especially considering the differences in the geometry of these experiments to the simulated circuit.

4. CONCLUSIONS

The present work can provide an useful tool for dimensioning of the natural circulation with liquids with heat generation, being especially useful for calculating the passive heat removal of Molten Salt Reactors. The lack of data for

natural circulation in asymmetrical circuits with heat generation meant that the closest correlations we could use were for rectangular circuits, and since our results were in accordance with those, we can conclude that these correlations could also be used as an estimation for our circuit. Since we did not study the effect of the Prandl number on the heat transfer, the correlation presented can only be applied to very specific problems, and thus the effect on the Prandt number should also be included in the correlation in order to broaden its application.

5. REFERENCES

A. P. S. Freire, A.I. and Colaço, M.J., 2006. *Turbulência*. ABCM, 1st edition.

Aufiero, M., 2014. "Development of an openfoam model for the molten salt fast reactor transientanalysis". *Chemical Engineering Science*, Vol. 111, pp. 390–401.

Barozzi, G., 2000. "Natural convection in cavities containing internal sources". *Heat and Mass Transfer*, Vol. 36, pp. 473–480.

Brovchenko, M., 2012. "Preliminary safety calculations to improve the design of molten salt fast reactor". *Proceedings of PHYSOR*, pp. 15–20.

IAEA, ed., 1991. *International Conference on the Safety of Nuclear Power : Strategy for the Future*, Proceedings series (International Atomic Energy Agency). UNIPUB.

Launder, B. and Spalding, D., 1974. *Computer Methods in Applied Mechanics and Engineering*, Vol. 3.

Nishikawa, H., 2015. "Detection of the chaotic flow instability in a natural convection loop using the recurrence plot analysis and the nonlinear prediction". *Bulletin of the JSME*, Vol. 10, No. 2.

6. RESPONSIBILITY NOTICE

The authors are the only responsible for the printed material included in this paper.